RSC Advances

PAPER

View Article Online
View Journal | View Issue

Cite this: *RSC Adv.*, 2025, **15**, 29811

Interactions of hypervalent IF_5 and XeF_4O molecules *via* σ-hole site with Lewis bases and anions: a comparative *ab initio* study

Mahmoud A. A. Ibrahim, *[abc] Asmaa M. M. Mahmoud,[a] Rehab R. A. Saeed,[a] Mohammed N. I. Shehata,[ad] Tamer Shoeib [d] and Jabir H. Al-Fahemi*[e]

Received 30th June 2025
Accepted 12th August 2025

DOI: 10.1039/d5ra04648c

rsc.li/rsc-advances

Interactions of hypervalent IF_5 and XeF_4O molecules within the square pyramidal geometry *via* σ-hole site with Lewis bases (LB = NH_3 and NCH) and anions (X^- = F^-, Cl^-, Br^-, and I^-) were comparatively investigated using *ab initio* methods. The energetic features outlined remarkable interaction (E_{int}) and binding (E_{bind}) energies for all complexes aligned from −5.65 to −91.02 kcal mol^{-1} and from −5.53 to −65.89 kcal mol^{-1}, respectively. More negative E_{int} and E_{bind} values were demonstrated for $XeF_4O\cdots LB$ complexes, compared to $IF_5\cdots LB$ complexes, along with nominal deformation energies for all complexes. Turning to $IF_5\cdots$ and $XeF_4O\cdots X^-$ complexes, E_{bind} demonstrated the proficiency of the latter complexes, which was in synchronic with the $V_{s,max}$ claims. On the contrary, $IF_5\cdots X^-$ complexes demonstrated higher negative E_{int} values in comparison to $XeF_4O\cdots X^-$ complexes, which may be attributed to the considerable favorable deformation energies relevant to the former complexes rather than the latter candidates. Moreover, the E_{int} and E_{bind} were disclosed to ameliorate in coincidence with the Lewis basicity strength as follows: $IF_5/XeF_4O\cdots NCH < \cdots NH_3 < \cdots I^- < \cdots Br^- < \cdots Cl^- < \cdots F^-$. Quantum theory of atoms in molecules/noncovalent interactions index observations affirmed that the interactions of IF_5/XeF_4O molecules *via* σ-hole site with NH_3 and NCH were characterized with open- and closed-shell nature, respectively, while the $IF_5/XeF_4O\cdots X^-$ complexes were characterized with the coordinative covalent nature. Symmetry-adapted perturbation theory results pinpointed the predominance of the inspected interactions with the electrostatic forces. The acquired results will be advantageous for the ubiquitous investigation of understanding the impact of geometrical deformation on the interactions of hypervalent molecules and their applications in diverse fields such as materials science and crystal engineering.

Introduction

σ-Hole interaction is one of the most common noncovalent interactions within the scientific community, due to its vital role in drug discovery,[1,2] crystal material,[3–7] supramolecular chemistry,[8,9] anion recognition,[10] biochemistry,[11,12] and catalysis.[13] σ-Hole interaction is characterized as an attractive interaction between an electron-deficient region that exists along the extension of a covalent σ-bond of group VI–VIII element-containing molecules (*i.e.*, σ-hole) and a nucleophile.[14,15] Accordingly, σ-hole interactions of group VI–VIII element-containing molecules were termed tetrel,[16,17] pnicogen,[18–21] chalcogen,[22–24] halogen,[25–28] and aerogen[29–31] bonds, respectively.

In the literature, σ-hole interactions were discerned to be greatly affected by diverse factors. Basically, several studies pinpointed that σ-hole interactions are affected by the atomic size of the σ-hole donor atom and the electron-withdrawing power of its attached atom/group within electrophilic molecules.[32,33] Furthermore, a significant impact of the Lewis basicity of the utilized nucleophilic molecules on the strength of σ-hole interactions was unveiled. Illustratively, pnicogen-containing molecules were addressed to interact with various types of nucleophiles, forming different-in-strength pnicogen bonding interactions with favorable ones when nucleophiles were anions (X^-) compared to the neutral Lewis bases (LB).[34,35] These outcomes could be explained owing to the noncovalent nature of σ-hole site-based interactions within pnicogen-containing molecules⋯LB complexes, while the investigated interactions were characterized with a coordinative covalent nature within pnicogen-containing molecules⋯X^- complexes.

The effect of geometrical deformation on the σ-hole size of hypervalent molecules upon the complexation process with an

[a]Computational Chemistry Laboratory, Chemistry Department, Faculty of Science, Minia University, Minia 61519, Egypt. E-mail: m.ibrahim@compchem.net
[b]Department of Engineering, College of Engineering and Technology, University of Technology and Applied Sciences, Nizwa 611, Sultanate of Oman
[c]School of Health Sciences, University of KwaZulu-Natal, Westville Campus, Durban 4000, South Africa
[d]Department of Chemistry, The American University in Cairo, New Cairo 11835, Egypt
[e]Department of Chemistry, Faculty of Science, Umm Al-Qura University, Makkah, 21955, Saudi Arabia. E-mail: jhfahemi@uqu.edu.sa

LB was also investigated.[36–38] Such a deformation effect was extensively studied in molecules within the trigonal bipyramidal geometry. In this context, the pnicogen-(ZF_5) and halogen-(XF_3O_2) containing molecules demonstrated a drastic geometrical deformation after their interaction with LBs.[37,38] On the other hand, a tiny response for the aerogen-(XF_2O_3) containing molecules within the trigonal bipyramidal geometry to the geometrical deformation was denoted; hence, lower interaction energies were perceived. These annotations indicated the effective role of geometrical deformation in enhancing the emerging interactions. In the same avenue, a paucity of studies concerned with investigating the deformation effect on the characteristics of molecules in square pyramidal geometry upon the complexation process was uncovered. A recent study declared that the complexation process of the halogen-containing molecule in square pyramidal geometry, such as IF_5, with LBs resulted in significant deformation energies;[37] however, the impact of deformation on the interactions of the aerogen-containing molecule, such as XeF_4O, with LBs has not been inspected yet.

In this respect, the propensity of hypervalent IF_5 and XeF_4O molecules in the square pyramidal geometry to interact *via* σ-hole site with LBs and X^- was minutely inspected. In that vein, the $IF_5\cdots$ and $XeF_4O\cdots LB/X^-$ complexes (where LB = NH_3 and NCH; X^- = F^-, Cl^-, Br^-, and I^-) were investigated. Moreover, the nucleophilicity effect on the strength of the investigated interactions was detailedly considered. The obtained observations would serve as a valuable milestone for elucidating the comprehensive role of geometrical deformation on the interactions of hypervalent molecules and their applications in anion recognition and crystal engineering.

Computational method

Ab initio calculations were implemented to investigate the interactions of the hypervalent IF_5 and XeF_4O molecules in square pyramidal geometry *via* σ-hole site with LB and X^- using Gaussian 09 program[39] (Fig. 1). In this context, NH_3 and NCH were designated as LBs, and F^-, Cl^-, Br^-, and I^- were picked as X^-. Accordingly, the MP2/aug-cc-pVTZ level of theory was utilized to geometrically optimize the inspected monomers and complexes.[40–44] The aug-cc-pVTZ-PP basis set was used for the I and Xe atoms to take the relativistic effects into account. The frequency computations were carried out for all optimized complexes, elucidating the true minima nature of all complexes except for the $IF_5\cdots NCH$ and $XeF_4O\cdots NH_3$ ones. EP analysis was conducted to identify the regions with electron-poor and electron-rich nature over the surface of chemical systems.[45–47] Based on the previous recommendations, an electron density contour of 0.002 a.u. was utilized owing to its worthy representation for the surfaces of chemical systems.[48,49] Consequently, the descriptive and numerical results of the electron density distributions over the entity of the chemical systems were performed by molecular electrostatic potential (MEP) maps and surface electrostatic potential extrema ($V_{s,max}/V_{s,min}$), respectively. Moreover, the electron localization function (ELF) analysis was executed to indicate the Lewis basicity affinity of the studied LB and X^-. In this context, ELF maps were generated to indicate the localized electron density region through visualizing the bonding pattern and lone pairs within the studied systems.

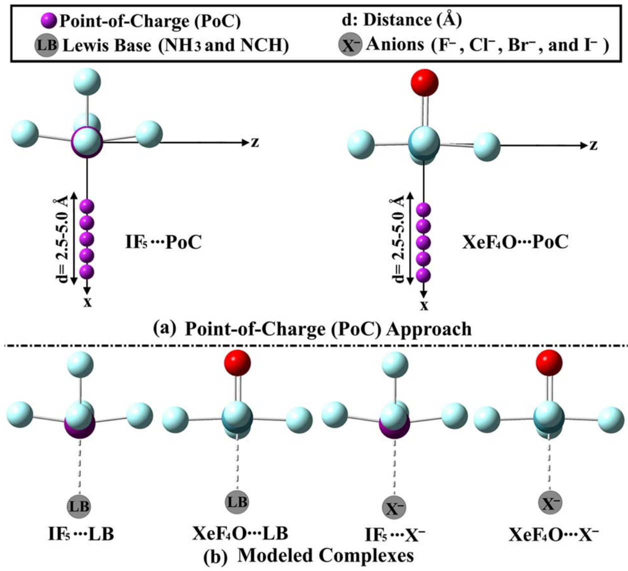

Fig. 1 Depictive representation for (a) PoC approach and (b) the modeled $IF_5\cdots$ and $XeF_4O\cdots LB/X^-$ complexes.

To evaluate the Lewis basicity effect from the electrostatic viewpoint, molecular stabilization of halogen- and aerogen-containing molecules in the presence of PoCs = −0.25, −0.50, −0.75, and −1.00 a.u. was inspected.[50] In this vein, molecular stabilization energy ($E_{stabilization}$) was calculated at I/Xe···PoC distance in the range from 2.5 to 5.0 with a step size of 0.1 Å according to eqn (1).[51]

$$E_{stabilization} = E_{molecule\cdots PoC} - E_{molecule} \quad (1)$$

Within the complexation process, interaction energy (E_{int}) for optimized $IF_5\cdots$ and $XeF_4O\cdots LB/X^-$ complexes was formulated as the difference between the total energy of the complex and the sum of its monomers correlated to their coordinates in the optimized complex. The binding energy (E_{bind}) was calculated as the difference between the total energy of the optimized complexes and the sum of the energies of isolated monomers.[52] Consequently, the deformation energy (E_{def}) was brought about by the complexation of the two interacting monomers and was yielded by subtracting the E_{int} from the E_{bind}.[53] Using the Boys-Bernard counterpoise correction method, the inherent basis set superposition error (BSSE) was eradicated from the aforementioned calculations.[54] The E_{int}, E_{bind}, and E_{def} of the studied complexes were explained in the following equations.

$$E_{int} = E_{IF_5/XeF_4O\cdots LB/X^-} - (E_{IF_5/XeF_4O\text{ in complex}} + E_{LB/X^-\text{in complex}}) + E_{BSSE} \quad (2)$$

$$E_{bind} = E_{IF_5/XeF_4O\cdots LB/X^-} - (E_{IF_5/XeF_4O} + E_{LB/X^-}) + E_{BSSE} \quad (3)$$

$$E_{def} = E_{bind} - E_{int} \quad (4)$$

The computed interaction energy at $E_{\text{MP2/aug-cc-pVTZ(PP)}}$ was benchmarked through the CCSD(T)/CBS computational level, depending on the subsequent equations.[55]

$$E_{\text{CCSD(T)/CBS}} = \Delta E_{\text{MP2/CBS}} + \Delta E_{\text{CCSD(T)}} \quad (5)$$

where

$$\Delta E_{\text{MP2/CBS}} = (64E_{\text{MP2/aug-cc-pVQZ}} - 27E_{\text{MP2/aug-cc-pVTZ}})/37 \quad (6)$$

$$\Delta E_{\text{CCSD(T)}} = E_{\text{CCSD(T)/aug-cc-pVDZ}} - E_{\text{MP2/aug-cc-pVDZ}} \quad (7)$$

In eqn (6), the 64 and 27 factors were driven from the well-established two-point X^{-3} extrapolation method, where the cardinal number (X) equals 4 and 3 for the aug-cc-pVQZ and aug-cc-pVTZ basis sets, respectively.[56] At the same time, the 37 factor represents the difference between the cube of the above-mentioned cardinal numbers. To qualitatively illustrate the nature of interactions within the $IF_5\cdots$ and $XeF_4O\cdots LB/X^-$ complexes, QTAIM and NCI index analyses were invoked.[57,58] By employing QTAIM, bond paths (BPs) and bond critical points (BCPs) were generated. Various topological properties such as potential energy density (V_b), electron density (ρ_b), Laplacian ($\nabla^2\rho_b$), lagrangian kinetic energy (G_b), total energy density (H_b), and the negative ratio of kinetic and potential electron energy density ($-G_b/V_b$) were assessed. The 2D reduced density gradient (RDG) and 3D colored NCI plots were also mapped. The $V_{s,max}$, $V_{s,min}$, ELF, QTAIM, and NCI analyses were carried out using the Multiwfn 3.7 package.[59] The schemes of QTAIM and NCI were portrayed using Visual Molecular Dynamics software.[60] SAPT calculations were executed as a vigorous method to dissect the essential physical components of the $E_{\text{SAPT2+(3)dMP2}}$ into electrostatic (E_{elst}), induction (E_{ind}), dispersion (E_{disp}), and exchange energies (E_{exch}) through eqn (8)–(12).[61,62] In this vein, SAPT upshots were computed at the SAPT2+(3)dMP2 truncation level using PSI4 code[63] for all the inspected complexes.

$$E_{\text{int}}^{\text{SAPT2+(3)dMP2}} = E_{\text{elst}} + E_{\text{ind}} + E_{\text{disp}} + E_{\text{exch}} \quad (8)$$

where

$$E_{\text{elst}} = E_{\text{elst}}^{(10)} + E_{\text{elst}}^{(12)} + E_{\text{elst}}^{(13)} \quad (9)$$

$$E_{\text{ind}} = E_{\text{ind,resp}}^{(20)} + E_{\text{exch-ind,resp}}^{(20)} + E_{\text{ind,resp}}^{(22)} + E_{\text{exch-ind,resp}}^{(22)} + \delta E_{\text{HF}}^{(2)} + \delta E_{\text{MP2}}^{(2)} \quad (10)$$

$$E_{\text{disp}} = E_{\text{disp}}^{(20)} + E_{\text{exch-disp}}^{(20)} + E_{\text{disp}}^{(21)} + E_{\text{disp}}^{(22)}(\text{SDQ}) + E_{\text{disp}}^{(22)}T + E_{\text{disp}}^{(30)} \quad (11)$$

$$E_{\text{exch}} = E_{\text{exch}}^{(10)} + E_{\text{exch}}^{(11)} + E_{\text{exch}}^{(12)} \quad (12)$$

Results

EP analysis

EP analysis was established to systematically outline the electron density distribution over the surface of the inspected IF_5 and XeF_4O molecules, along with LBs and X^-. Fig. 2 portrays the MEP maps along with $V_{s,max}$ and $V_{s,min}$ values of the optimized IF_5, XeF_4O, LBs, and X^- molecules.

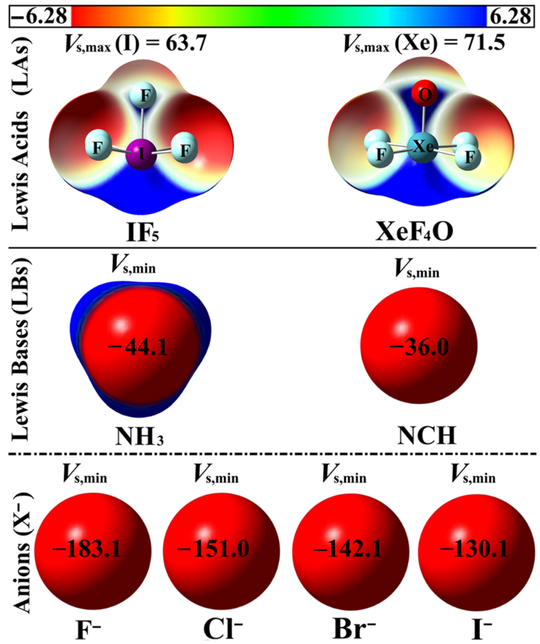

Fig. 2 Molecular electrostatic potential maps of the investigated IF_5 and XeF_4O molecules as Lewis acids, along with the utilized LB and X^- using 0.002 a.u. electron density isosurface. MEP scale varies from −6.28 (red) to 6.28 (blue) kcal mol^{-1}.

As displayed in Fig. 2, for the Lewis acid centers, σ-hole was found at the outer surface of I and Xe atoms of the IF_5 and XeF_4O molecules, respectively. In this context, a larger σ-hole was denoted for the XeF_4O molecule rather than the IF_5 candidate, outlining an elevated potency for the former molecule to engage in favorable interactions *via* σ-hole site compared to the latter one. In coincidence with the MEP claims, the paramount $V_{s,max}$ values were evaluated, showing values up to 63.7 and 71.5 kcal mol^{-1} for IF_5 and XeF_4O molecules, respectively.

Regarding the studied LBs, the surface of the N atom within the NH_3 and NCH molecules was decorated with red negative sites with $V_{s,min}$ values of −44.1 and −36.0 kcal mol^{-1}, respectively. Moreover, the entity of X^- was entirely covered with red color as a result of its full negative charge. It was also noted that the extent of anions' charge was discerned to diminish by increasing their atomic size, giving $V_{s,min}$ values amounting to −183.1, −151.0, −142.1, and −130.1 kcal mol^{-1} for F^-, Cl^-, Br^-, and I^-, respectively. Comparatively, the X^- anions were detected with a higher discriminatory nucleophilic nature over the inspected LBs.

ELF analysis

ELF analysis provides a topological framework illustrating the localized electron density regions in atoms and molecules, with the objective of elucidating the chemical reactivity of chemical systems.[64,65] Accordingly, the ELF maps were generated for the studied LB and X^- and are displayed in Fig. 3.

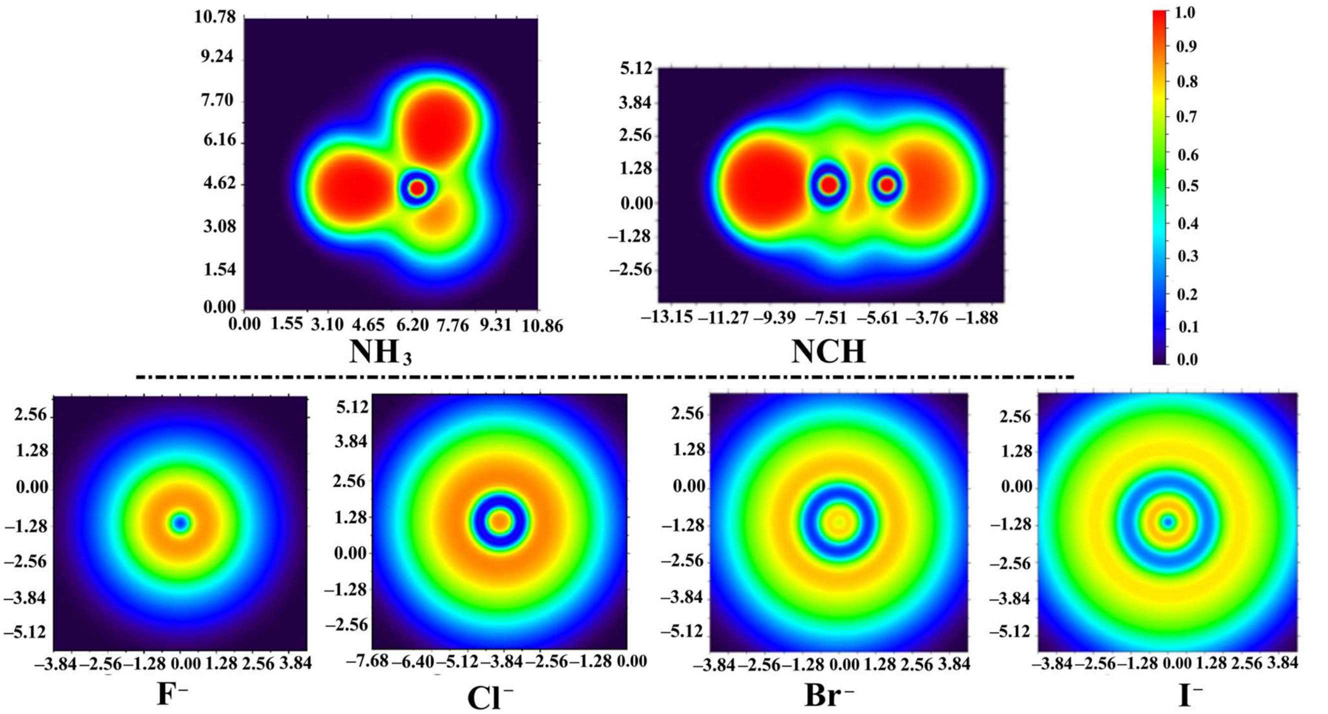

Fig. 3 ELF maps of the studied LBs and X^-. The red (ELF = 1) and blue (ELF = 0) show the localized and delocalized electron density regions, respectively. The coordinates are expressed in bohr.

From Fig. 3, a red lobe (*i.e.*, free lone pair basin) was observed over the NH_3 and NCH molecules. The tight and compact nature of this basin indicated the confinement of the lone pair electrons owing to the elevated electronegativity character of the N atom. Turning to the studied X^-, the ELF map of F^- demonstrated a small and dense red region near the nucleus surrounded by tightly packed rings, pinpointing the highly localized core electrons and compact free electron pair basins. These findings outlined the high Lewis basicity character of the F^-. Notably, the red regions were found to expand radially outward, and the ELF basins became broader on going from Cl^- to Br^- and I^-, indicating the retreating of Lewis basicity character.

PoC calculations

Towards more illustration of the propensity of the studied chemical systems (*i.e.*, IF_5 and XeF_4O) to electrostatically form noncovalent interactions, the PoC approach was implemented.[66] In PoC context, negatively-charged PoC with values of −0.25, −0.50, −0.75, and −1.00 a.u. were used to imitate the Lewis basicity effect on the studied interactions.[51] The

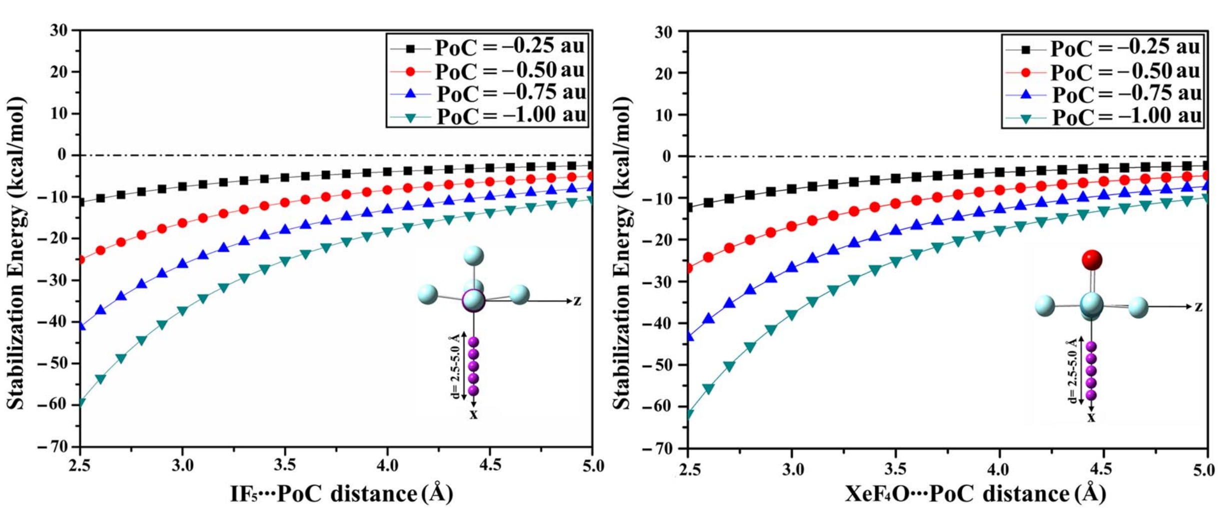

Fig. 4 Molecular stabilization energy curves of the $IF_5\cdots$ and $XeF_4O\cdots$PoC systems.

Table 1 $E_{stabilization}$ of $IF_5\cdots$ and $XeF_4O\cdots$PoC systems at I/Xe⋯PoC distance of 2.5 Å

	Molecular stabilization energy (kcal mol^{-1})			
Systems	PoC = −0.25 a.u.	PoC = −0.50 a.u.	PoC = −0.75 a.u.	PoC = −1.00 a.u.
$IF_5\cdots$PoC	−11.31	−25.13	−41.17	−59.22
$XeF_4O\cdots$PoC	−12.30	−26.82	−43.33	−61.70

molecular stabilization energy curves of the $IF_5\cdots$ and $XeF_4O\cdots$PoC systems were created and are portrayed in Fig. 4, and their $E_{stabilization}$ at I/Xe⋯PoC distance of 2.5 Å are gathered in Table 1.

As evident in Fig. 4, a significant potency for the IF_5 and XeF_4O molecules to engage in favorable interactions *via* σ-hole site was detected by obtaining negative $E_{stabilization}$ values for all IF_5 and XeF_4O molecules in the presence of negative PoC. Further, $E_{stabilization}$ curves were noted to augment simultaneously with the negativity of PoC, showing the proficient role of the nucleophilicity in the favorability of the noncovalent interactions. Further, the $E_{stabilization}$ was detected to decrease by increasing the I/Xe⋯PoC distance.

The collected data in Table 1 demonstrated that a considerable increment of $E_{stabilization}$ was harmonically in line with elevating the negative PoC values. For example, $E_{stabilization}$ values for $IF_5\cdots$PoC systems were −11.31, −25.13, −41.17, and −59.22 kcal mol^{-1} with PoCs of −0.25, −0.50, −0.75, and −1.00 a.u., respectively. Obviously, a direct correlation was observed between EP claims and PoC ones. Evidently, more preferential $E_{stabilization}$ outcomes were disclosed for the $IF_5\cdots$PoC systems compared to the $XeF_4O\cdots$PoC candidates. For instance, in the being of PoC = −0.25 a.u., $E_{stabilization}$ was disclosed to be −11.31 and −12.30 kcal mol^{-1} for $IF_5\cdots$ and $XeF_4O\cdots$PoC systems along with $V_{s,max}$ of 63.7 and 71.5 kcal mol^{-1} for IF_5 and XeF_4O molecules, respectively.

Geometrical structure and stability

Interactions of IF_5 and XeF_4O molecules *via* σ-hole site with LBs and X^- were investigated. The optimized structures of $IF_5\cdots$ and $XeF_4O\cdots LB/X^-$ complexes are portrayed in Fig. 5, and their related E_{bind}, E_{int}, E_{def}, and $E_{CCSD(T)/CBS}$ are included in Table 2.

As evident in Fig. 5, optimized structures were obtained for all complexes, indicating the potency of the IF_5 and XeF_4O molecules within the square pyramidal geometry to interact favorably *via* σ-hole site with the studied LBs and X^-. The inspected interactions were characterized with a highly directional character where all F–I⋯N and O–Xe⋯N angles within the optimized complexes were nearly equal to 180°, except for $IF_5\cdots NH_3$ one. The F–I⋯N angle within the $IF_5\cdots NH_3$ complex was identified to be nearly 141.43°, which was in synchronic with the previous reports.[37]

From Table 2, a boosting in the F–I and O–Xe intra-molecular distances (d_1) was uncovered after the interaction of IF_5 and XeF_4O molecules with X^-. In contrast, negligible changes in the d_1 were found in the case of interactions with LBs. With respect to the inter-molecular distances (d_2), they were found to be shorter and longer than the sum of the vdW and covalent radii, respectively (Table 2).

Regarding $IF_5\cdots$ and $XeF_4O\cdots$LB complexes, negative E_{int} and E_{bind} values were denoted with higher preferentiality for the latter complexes rather than the former candidates, indicating

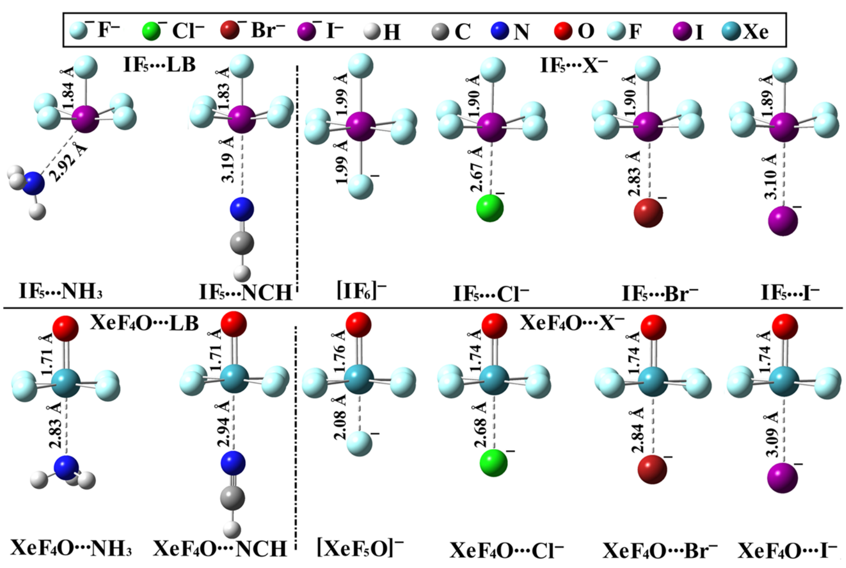

Fig. 5 Structures of the optimized $IF_5\cdots$ and $XeF_4O\cdots LB/X^-$ complexes accompanied by their F–I and O–Xe intra (d_1)- and I/Xe⋯LB/X^- inter (d_2)-molecular distances in Å.

Table 2 Complexation parameters of the optimized $IF_5\cdots$ and $XeF_4O\cdots LB/X^-$ complexes. Energies, distances, and angles are in kcal mol^{-1}, Å, and °, respectively

	Distances					Energies			
Complexes	d_1[a]	d_2[b]	$\sum r_{vdW}$[c]	$\sum r_{covalent}$[c]	Angle	E_{bind}	E_{int}	$E_{CCSD(T)/CBS}$	E_{def}
$IF_5\cdots NH_3$	1.84	2.92	3.53	2.08	141.43	−8.87	−9.30	−10.28	0.43
$IF_5\cdots NCH$	1.83	3.19	3.53	2.08	179.99	−5.53	−5.65	−6.00	0.12
$[IF_6]^-$	1.99	1.99	3.45	2.04	179.99	−64.72	−91.02	−94.76	26.30
$IF_5\cdots Cl^-$	1.90	2.67	3.73	2.39	180.00	−35.46	−45.05	−47.00	9.59
$IF_5\cdots Br^-$	1.90	2.83	3.83	2.61	180.00	−33.59	−40.37	−42.11	6.78
$IF_5\cdots I^-$	1.89	3.10	3.96	2.80	180.00	−28.21	−33.64	−35.41	5.43
$XeF_4O\cdots NH_3$	1.71	2.83	3.71	2.18	179.95	−11.42	−12.06	−11.97	0.64
$XeF_4O\cdots NCH$	1.71	2.94	3.71	2.18	179.87	−7.89	−8.04	−7.75	0.15
$[XeF_5O]^-$	1.76	2.08	3.63	2.14	179.99	−65.89	−74.21	−72.26	8.32
$XeF_4O\cdots Cl^-$	1.74	2.68	3.91	2.49	179.99	−40.59	−44.57	−43.33	3.98
$XeF_4O\cdots Br^-$	1.74	2.84	4.01	2.71	179.99	−36.19	−39.94	−38.77	3.75
$XeF_4O\cdots I^-$	1.74	3.09	4.14	2.90	179.99	−30.43	−33.65	−33.02	3.22

[a] d_1 represents the F–I and O–Xe intra-molecular distances that are equal to 1.83 and 1.71 Å for the isolated systems, respectively. [b] d_2 represents the I/Xe$\cdots$LB/X^- inter-molecular distance. [c] $\sum r_{vdW}$ and $\sum r_{covalent}$ represent the sum of van der Waals and covalent radii of the interacting atoms, respectively.

the occurrence of favorable interactions between the interacting species (Table 2). Notably, the energetic features were in line with the EP upshots. Illustratively, E_{bind}/E_{int} values were −11.42/−12.06 and −8.87/−9.30 kcal mol^{-1} for $IF_5\cdots$ and $XeF_4O\cdots NH_3$ complexes, accompanied by $V_{s,max}$ values of 63.7 and 71.5 kcal mol^{-1} for IF_5 and XeF_4O molecules, respectively. Moreover, negligible geometrical deformation was denoted for all $IF_5\cdots$ and $XeF_4O\cdots$LB complexes where E_{def} values were aligned in the range from 0.12 to 0.64 kcal mol^{-1}.

Turning to $IF_5\cdots$ and $XeF_4O\cdots X^-$ complexes, a direct correlation was noted between the E_{bind}/E_{int} upshots and the $V_{s,max}$ claims. Clearly, more negative E_{bind} values were disclosed for $XeF_4O\cdots X^-$ complexes than the $IF_5\cdots X^-$ complexes, while higher negative E_{int} values were observed in the case of the latter complexes than the former one. For instance, E_{bind} and E_{int} were computed to be −35.46/−40.59 and −45.05/−44.57 kcal mol^{-1} for $IF_5/XeF_4O\cdots Cl^-$ complexes, accompanied by $V_{s,max}$ values of 63.7 and 71.5 kcal mol^{-1} for IF_5 and XeF_4O molecules, respectively. This finding could be explained by observing higher deformation energies in the case of $IF_5\cdots X^-$ complexes (E_{def} = 5.43–26.30 kcal mol^{-1}) than the $XeF_4O\cdots X^-$ candidates (E_{def} = 3.22–8.32 kcal mol^{-1}). Generally, the considerable E_{bind} and E_{int} relevant to the $IF_5/XeF_4O\cdots X^-$ complexes declared the formation of coordinative covalent bonds, as previously documented.[35] It is worth mentioning that the extremely high E_{bind}/E_{int} of the $IF_5\cdots$ and $XeF_4O\cdots F^-$ complexes uncovered the formation of I–F^- and Xe–F^- covalent bonds and hence the $[IF_6]^-$ and $[XeF_5O]^-$ molecules were obtained.

Notably, a direct correlation between MP2 energies of $IF_5\cdots$ and $XeF_4O\cdots LB/X^-$ complexes and the nucleophilicity of the studied LBs. The E_{bind} and E_{int} values were denoted to increase with increasing nucleophilicity of the studied LBs as follows: $IF_5/XeF_4O\cdots NCH < \cdots NH_3 < \cdots I^- < \cdots Br^- < \cdots Cl^- < \cdots F^-$ complexes. This finding could be explained due to increasing the attractive forces between the positive regions relevant to the IF_5/XeF_4O molecules (*i.e.*, σ-hole site) and the negative portions of the studied LBs and X^-. For example, E_{int} values of $IF_5\cdots Cl^-$, $\cdots Br^-$, $\cdots I^-$, $\cdots NH_3$ and $\cdots$NCH complexes were −45.05, −40.37, −33.64, −9.30 and −5.65 kcal mol^{-1} along with $V_{s,min}$ values of −183.1 and −151.0, −142.1, −130.1, −44.1, −36.0 kcal mol^{-1} for F^-, Cl^-, Br^-, I^-, NH_3, and NCH molecules. Clearly, this observation was also in coincidence with the PoC claims (Table 1/Fig. 2).

Noteworthy, the energetic results at the CCSD(T)/CBS level of theory showed similar trends with the outcomes related to the MP2/aug-cc-PVTZ(PP) counterparts. For instance, $E_{CCSD(T)/CBS}$ values were −47.00 and −43.33 kcal mol^{-1}, along with E_{bind}/E_{int} of −35.46/−45.05 and −40.59/−44.57 kcal mol^{-1} for $IF_5\cdots$ and $XeF_4O\cdots Cl^-$ complexes, respectively.

QTAIM analysis

Quantum theory of atoms in molecules (QTAIM), established by Bader *et al.*,[57] is regarded as a reliable method for providing comprehensive insights into the nature of intermolecular interactions.[67] Therefore, QTAIM analysis was herein conducted for $IF_5\cdots LB/X^-$ and $XeF_4O\cdots LB/X^-$ containing complexes. Fig. 6 delineates the QTAIM portrays of $IF_5\cdots$ and $XeF_4O\cdots LB/X^-$ complexes, and Table 3 lists the relevant topological parameters along the corresponding bond paths and bond critical points.

As manifested in Fig. 6, single BCP and BP within the optimized $IF_5\cdots$ and $XeF_4O\cdots LB/X^-$ complexes were observed, which in turn confirmed the occurrence of attractive interactions between the interacting species. Clearly, for $IF_5/XeF_4O\cdots$LB complexes, more positive ρ_b and $\nabla^2\rho_b$ along with more negative H_b and V_b values were recorded when LB = NH_3 compared to NCH. Moreover, values of $-G_b/V_b$ were found to be lower and higher than unity for the $IF_5/XeF_4O\cdots NH_3$ and $\cdots$NCH complexes (Table 3), respectively. These findings announced the open- and closed-shell nature of the studied interactions within the $IF_5/XeF_4O\cdots NH_3$ and $\cdots$NCH complexes,

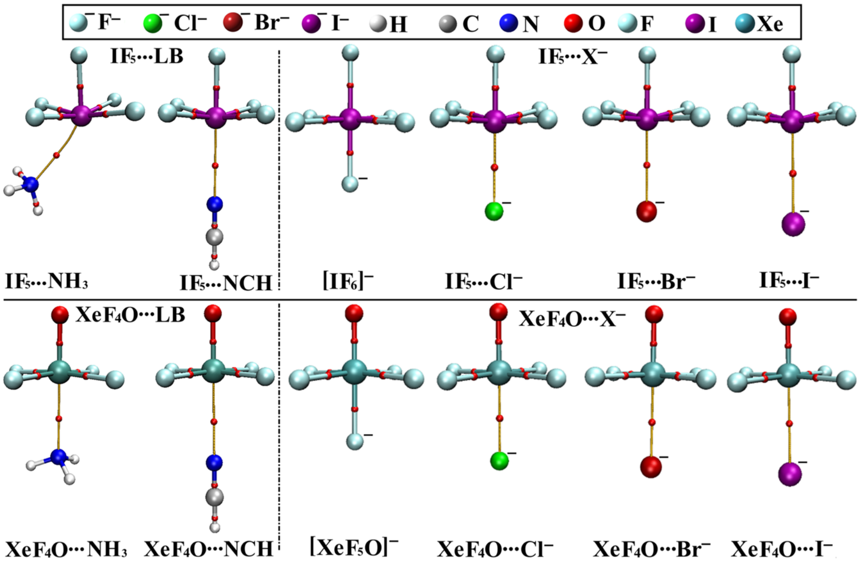

Fig. 6 QTAIM scheme of the optimized $IF_5\cdots$ and $XeF_4O\cdots LB/X^-$ complexes.

Table 3 The QTAIM parameters of the optimized $IF_5\cdots$ and $XeF_4O\cdots LB/X^-$ complexes

Complex	ρ_b	$\nabla^2\rho_b$	H_b	G_b	V_b	$-G_b/V_b$
$IF_5\cdots NH_3$	0.0244	0.0610	−0.0001	0.0154	−0.0155	0.9914
$IF_5\cdots NCH$	0.0140	0.0445	0.0016	0.0095	−0.0078	1.2081
$[IF_6]^-$	0.1235	0.2859	−0.0615	0.1329	−0.1944	0.6838
$IF_5\cdots Cl^-$	0.0578	0.0868	−0.0137	0.0354	−0.0492	0.7207
$IF_5\cdots Br^-$	0.0504	0.0698	−0.0100	0.0275	−0.0375	0.7324
$IF_5\cdots I^-$	0.0398	0.0489	−0.0064	0.0187	−0.0251	0.7435
$XeF_4O\cdots NH_3$	0.0317	0.0807	−0.0012	0.0214	−0.0226	0.9459
$XeF_4O\cdots NCH$	0.0216	0.0705	0.0014	0.0163	−0.0149	1.0916
$[XeF_5O]^-$	0.1090	0.2578	−0.0458	0.1206	−0.1855	0.6501
$XeF_4O\cdots Cl^-$	0.0577	0.1000	−0.0127	0.0377	−0.0503	0.7483
$XeF_4O\cdots Br^-$	0.1348	0.2292	−0.0751	0.1324	−0.2075	0.6381
$XeF_4O\cdots I^-$	0.0407	0.0526	−0.0068	0.1345	−0.2114	0.6364

respectively. Illustratively, ρ_b, $\nabla^2\rho_b$, H_b, V_b, and $-G_b/V_b$ values of $XeF_4O\cdots NH_3/NCH$ complexes were 0.0317/0.0216, 0.0807/0705, −0.0012/0.0014, −0.0226/−0.0149, and 0.9459/1.0916 a.u., respectively. Accordingly, among the investigated complexes, only $IF_5\cdots$ and $XeF_4O\cdots NCH$ complexes exhibited true halogen and aerogen bonds, respectively.

With respect to $IF_5\cdots$ and $XeF_4O\cdots X^-$ complexes, the topological parameters generally demonstrated an increase in the coordinative covalent nature of the studied interactions on going from $X^- = I^-$ to Br^-, Cl^-, and F^- due to the following annotations: more negative values of H_b and V_b along with more positive ρ_b and $\nabla^2\rho_b$ values whereas the $-G_b/V_b$ were found to be less than unity. For example, the ρ_b, $\nabla^2\rho_b$, H_b, V_b, and $-G_b/V_b$ values of $IF_5\cdots Br^-/Cl^-$ were 0.0504/0.0578, 0.0698/0.0868, −0.0100/−0.0137, −0.0375/0.0492, and 0.7324/0.7207 a.u., respectively.

Generally, all the topological parameters coincided with the energetic patterns for all the complexes under investigation. Illustratively, the topological parameters outlined the preference of the $IF_5/XeF_4O\cdots X^-$ complexes over the $IF_5/XeF_4O\cdots LBs$ candidates, which was in synchronic with the energetic findings. For instance, ρ_b values were 0.0244/0.1235 and 0.0317/0.1090 a.u. accompanied by E_{int} of −9.30/−91.02 and −12.06/−74.21 kcal mol^{-1} for $IF_5\cdots$ and $XeF_4O\cdots NH_3/F^-$ complexes, respectively.

NCI-RDG analysis

The NCI-RDG index is documented as a punctilious tool to delicately indicate the nature of intermolecular interactions.[58] Fig. 7 shows the 2D and 3D NCI plots for the optimized $IF_5\cdots$ and $XeF_4O\cdots LB/X^-$ complexes. In 3D NCI plots, the color scale of the isosurfaces ranged from green (*i.e.*, noncovalent nature) to the blue (*i.e.*, covalent nature).

With respect to the studied complexes, all spikes in the RDG plots were shifted towards a more negative $(\lambda_2)\rho$ sign (*i.e.*, broader), along with ameliorating the interaction energies (Fig. 7). For example, in the case of $IF_5/XeF_4O\cdots X^-$ complexes, spikes became broader on going from $X^- = I^-$, to Br^-, Cl^-, and F^-. Regarding the 3D NCI plots, the appearance of green-coded surfaces within the $IF_5/XeF_4O\cdots NCH$ complexes outlined the noncovalent character of the investigated interactions. While in the case of the $IF_5/XeF_4O\cdots NH_3$ complexes, green-bluish surfaces were noticed, announcing the partial covalent nature of the emerging interactions. Besides, for the $IF_5\cdots NH_3$ complex, green isosurface was also observed between the F atom of IF_5 and the H atom of NH_3, announcing the role of $F\cdots H$ attractive interactions in stabilizing the $IF_5\cdots NH_3$ complex. On the other side, a blue isosurface region was recorded within the $IF_5\cdots$ and $XeF_4O\cdots X^-$ complexes, pinpointing the existence of maximal attractive forces (*i.e.*, coordinative covalent nature) between the interacting molecules.

Remarkably, QTAIM and NCI upshots were significantly consistent with the energy upshots, clarifying the potency of the considered molecules to form varied-in-strength interactions

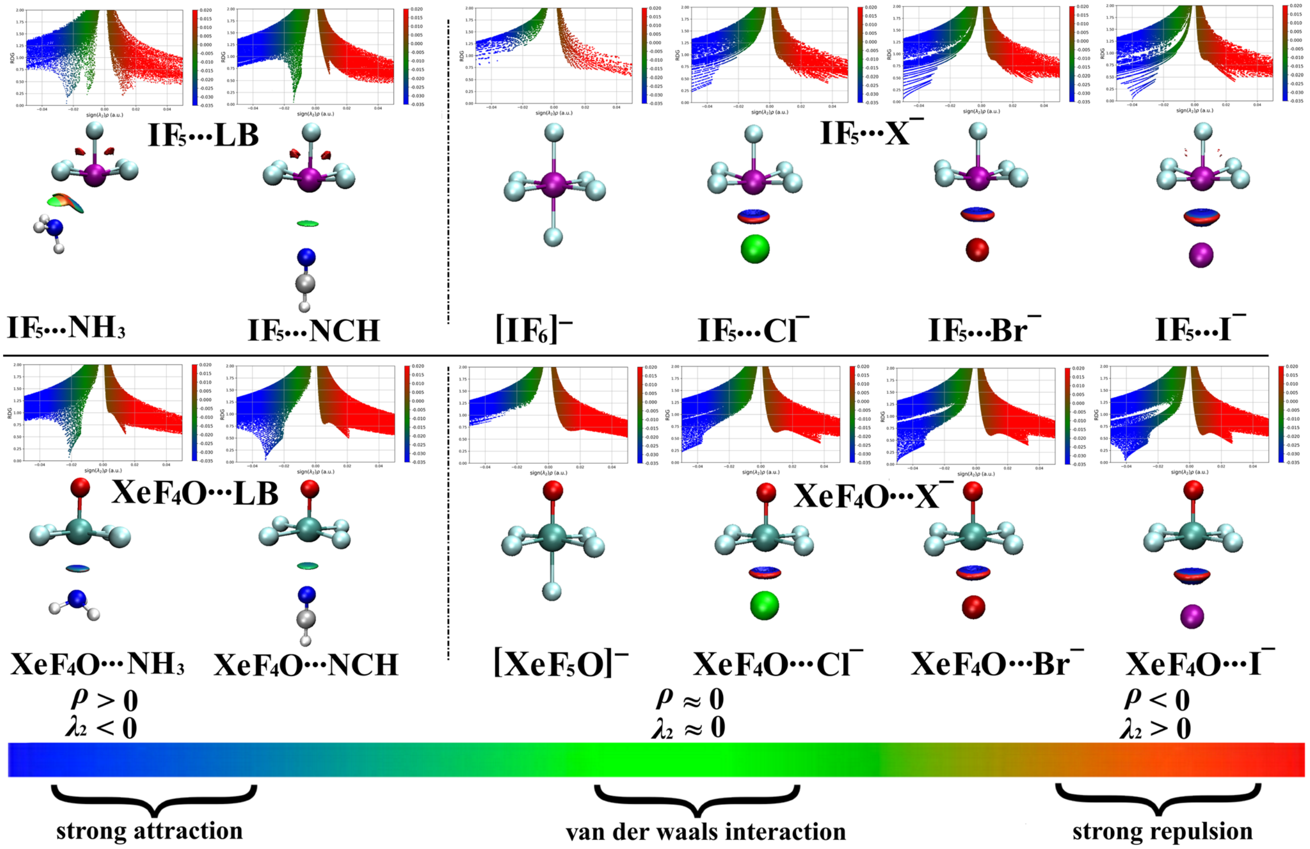

Fig. 7 2D and 3D NCI diagrams for the optimized $IF_5\cdots$ and $XeF_4O\cdots LB/X^-$ complexes depending on the sign $(\lambda_2)\rho$.

via σ-hole site depending on the nature of the nucleophilic system.

SAPT calculations

SAPT method was herein employed to energetically elaborate the forces that contribute to the inter-molecular interactions within the optimized $IF_5\cdots$ and $XeF_4O\cdots LB/X^-$ complexes.[68] Table 4 illustrates the attractive and repulsive energetic components along with the total SAPT2+(3)dMP2 energy for optimized $IF_5\cdots$ and $XeF_4O\cdots LB/X^-$ complexes.

Among all the attractive energetic forces, the E_{elst} was observed as the dominant component for all optimized complexes, as demonstrated in Fig. 8. The E_{disp} and E_{ind} were denoted with different contributions within all $IF_5/XeF_4O\cdots LB$ and $\cdots X^-$ complexes. This observation outlined the attractive nature of such forces and hence their contributions in stabilizing the investigated complexes. On the other hand, positive

Table 4 E_{elst}, E_{ind}, E_{disp}, E_{exch}, and $E_{SAPT2+(3)dMP2}$ along with the energy difference ($\Delta\Delta E$) between the MP2 and SAPT2+(3)dMP2 energies of the optimized $IF_5\cdots$ and $XeF_4O\cdots LB/X^-$ complexes. All energies are in kcal mol^{-1}

Complex	E_{elst}	E_{ind}	E_{disp}	E_{exch}	$E_{SAPT2+(3)dMP2}$ [a]	$\Delta\Delta E$ [b]
$IF_5\cdots NH_3$	−18.92	−5.54	−6.42	21.15	−9.98	−0.68
$IF_5\cdots NCH$	−7.87	−1.91	−3.02	7.12	−5.68	−0.03
$[IF_6]^-$	−158.25	−118.45	−24.63	204.26	−97.07	−6.05
$IF_5\cdots Cl^-$	−73.45	−42.74	−15.00	84.63	−46.55	−1.50
$IF_5\cdots Br^-$	−62.67	−38.64	−14.61	73.84	−42.09	−1.72
$IF_5\cdots I^-$	−50.69	−30.69	−13.19	59.49	−35.09	−1.45
$XeF_4O\cdots NH_3$	−22.91	−8.14	−6.81	25.54	−12.32	−0.26
$XeF_4O\cdots NCH$	−11.71	−3.69	−4.74	12.17	−7.98	0.06
$[XeF_5O]^-$	−131.70	−84.42	−20.80	157.14	−79.79	−5.58
$XeF_4O\cdots Cl^-$	−69.83	−39.23	−15.26	77.74	−46.58	−2.01
$XeF_4O\cdots Br^-$	−60.76	−35.89	−15.10	69.78	−41.97	−2.03
$XeF_4O\cdots I^-$	−50.27	−29.80	−14.15	58.85	−35.37	−1.72

[a] $E_{SAPT2+(3)dMP2} = E_{ind} + E_{exch} + E_{elst} + E_{disp}$. [b] $\Delta\Delta E = E_{MP2/aug\text{-}cc\text{-}pVTZ(PP)} - E_{SAPT2+(3)dMP2}$.

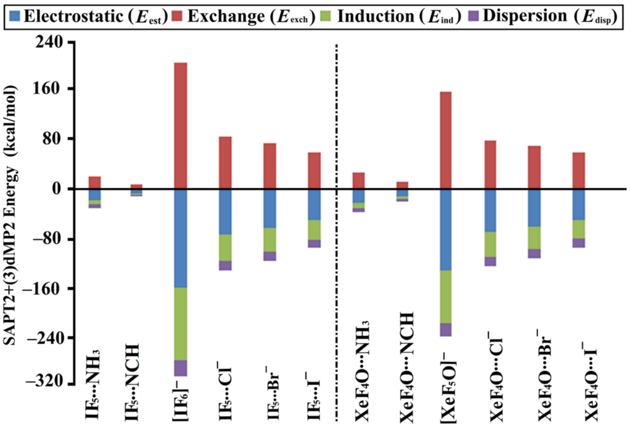

Fig. 8 Bar chart of SAPT energetic component for the optimized $IF_5\cdots$ and $XeF_4O\cdots LB/X^-$ complexes.

values of E_{exch} proclaimed the repulsive nature of such forces. For instance, E_{elst}, E_{ind}, E_{disp}, and E_{exch} were −73.45, −42.74, −15.00, and 84.63 kcal mol^{-1}.

According to data tabulated in Table 4, negative values for the $E_{elst}/E_{disp}/E_{ind}$ components were disclosed, unveiling their attractive nature. On the other hand, unfavorable positive E_{exch} values were found for all complexes, pinpointing the repulsive nature of E_{exch}. Among the attractive forces, the electrostatics were the predominant attractive forces within all the $IF_5\cdots$ and $XeF_4O\cdots LB/X^-$ complexes. Generally, the attractive energetic components for $IF_5\cdots$ and $XeF_4O\cdots LB$ complexes were ordered as follows: $E_{ind} < E_{disp} < E_{elst}$. For instance, E_{elst}, E_{disp}, and E_{ind} values were −18.92, −6.42, and −5.54 kcal mol^{-1} for $IF_5\cdots NH_3$ complex. For the $IF_5/XeF_4O\cdots X^-$ complexes, the attractive forces were denoted to increase in the following $E_{disp} < E_{ind} < E_{elst}$ sequence. For example, E_{elst}, E_{ind}, and E_{disp} were −69.83, −39.23, and −15.26 kcal mol^{-1} for $XeF_4O\cdots Cl^-$ complex, respectively. Basically, the variation in the trends relevant to the attractive forces could be attributed to the high ability of X^- compared to the LBs to polarize the σ-hole of IF_5/XeF_4O molecules more favorably.[51,69]

Clearly, great compatibility between SAPT-based results and MP2 energy-based counterparts. Illustratively, for $XeF_4O\cdots X^-$ complexes, the negative E_{elst}, E_{ind}, and E_{disp} values were observed to increase on going from $X^- = I^- < Br^- < Cl^- < F^-$. For instance, $E_{elst}/E_{ind}/E_{disp}$ of $XeF_4O\cdots I^-$, $\cdots Br^-$, $\cdots Cl^-$, and $\cdots F^-$ complexes were −50.27/−29.80/−14.15, −60.76/−35.89/−15.10, −69.83/−39.23/−15.26, and −131.70/−84.24/−20.80 kcal mol^{-1}, respectively. Moreover, SAPT results were in agreement with the QTAIM and NCI claims. Evidently, the coordinative covalent nature of the $IF_5\cdots$ and $XeF_4O\cdots X^-$ complexes was also confirmed by observing significant negative E_{elst}, E_{ind}, and E_{disp} values. Overall, the low values of $\Delta\Delta E$ ensured the reliability of the selected SAPT level (Table 4).

Conclusion

The tendency of the hypervalent IF_5 and XeF_4O molecules within the square pyramidal geometry to interact *via* σ-hole site with Lewis bases (LB = NH_3 and NCH) and anions (X^- = F^-, Cl^-, Br^-, and I^-) was inspected. For all $IF_5\cdots$ and $XeF_4O\cdots LB/X^-$ complexes, significant interaction and binding (*i.e.*, E_{int} and E_{bind}, respectively) energies were detected in the range from −5.65 to −91.02 kcal mol^{-1} and from −5.53 to −65.89 kcal mol^{-1}, respectively. Clearly, more negative E_{int} and E_{bind} values for the $XeF_4O\cdots LB$ complexes were noticed compared to the $IF_5\cdots LB$ candidates, outlining the preferentiality of the former complexes over the latter ones. In addition, all $IF_5\cdots$ and $XeF_4O\cdots LB$ complexes were characterized by meager deformation energies. Regarding $IF_5\cdots$ and $XeF_4O\cdots X^-$ complexes, E_{bind} declared that the anterior complexes were more favorable than posterior candidates, whereas the *vice versa* observations were noted in the case of E_{int} values. This annotation could be explained as an upshot of the significant deformation energies in the 5.43–26.30 kcal mol^{-1} energetic ambit for the $IF_5\cdots X^-$ complexes *versus* 3.22–8.32 kcal mol^{-1} one for the $XeF_4O\cdots X^-$ counterparts. Moreover, the energy features were noted to increase in line with the Lewis basicity strength as follows: $IF_5/XeF_4O\cdots NCH < \cdots NH_3 < \cdots I^- < \cdots Br^- < \cdots Cl^- < \cdots F^-$ complexes. QTAIM and NCI results announced that the interactions between the IF_5/XeF_4O molecules *via* σ-hole site with the NH_3 and NCH were characterized with the open- and closed-shell nature, respectively. In comparison, the $IF_5/XeF_4O\cdots X^-$ complexes were generally characterized by the coordinative covalent nature. SAPT upshots outlined that the driving force behind the occurrence of the inspected interactions was the electrostatic one. These results will help facilitate the comprehension of the investigated interactions and pave the way for several future applications in material science and crystal engineering fields.

Author contributions

Mahmoud A. A. Ibrahim: conceptualization, methodology, software, resources, project administration, supervision, writing—review and editing. Asmaa M. M. Mahmoud: data curation, formal analysis, investigation, visualization, writing—original draft. Rehab R. A. Saeed: methodology, investigation, project administration, writing—review and editing. Mohammed N. I. Shehata: methodology, investigation, project administration, writing—review and editing. Tamer Shoeib: software, resources, writing—review and editing. Jabir H. Al-Fahemi: resources, project administration, writing—review and editing.

Conflicts of interest

The authors declare that they have no known competing financial interests or personal relationships that could have appeared to influence the work reported in this paper.

Data availability

The data supporting this article have been included as part of the SI. See DOI: **https://doi.org/10.1039/d5ra04648c**.

Acknowledgements

The authors extend their appreciation to Umm Al-Qura University, Saudi Arabia for funding this research work through grant number: 25UQU4200274GSSR04.

References

1 Y. Lu, Y. Wang and W. Zhu, *Phys. Chem. Chem. Phys.*, 2010, **12**, 4543–4551.
2 Y. Lu, Y. Liu, Z. Xu, H. Li, H. Liu and W. Zhu, *Expert Opin. Drug Discovery*, 2012, **7**, 375–383.
3 K. T. Mahmudov, M. N. Kopylovich, M. F. C. Guedes da Silva and A. J. L. Pombeiro, *Dalton Trans.*, 2017, **46**, 10121–10138.
4 G. Berger, K. Robeyns, J. Soubhye, R. Wintjens and F. Meyer, *CrystEngComm*, 2016, **18**, 683–690.
5 M. Saccone, G. Cavallo, P. Metrangolo, G. Resnati and A. Priimagi, in *Halogen Bonding II: Impact on Materials Chemistry and Life Sciences*, ed. P. Metrangolo and G. Resnati, Springer International Publishing, Cham, 2015, pp. 147–166, DOI: 10.1007/128_2014_615.
6 C. Präsang and D. W. Bruce, *Helv. Chim. Acta*, 2023, **106**, e202300008.
7 P. Politzer, J. Murray, G. Janjić and S. Zarić, *Crystals*, 2014, **4**, 12–31.
8 D. A. Uhlenheuer, K. Petkau and L. Brunsveld, *Chem. Soc. Rev.*, 2010, **39**, 2817–2826.
9 D. K. Smith, *J. Chem. Educ.*, 2005, **82**, 393–400.
10 J. Y. C. Lim and P. D. Beer, *Chem*, 2018, **4**, 731–783.
11 K. Kriz, J. Fanfrlik and M. Lepsik, *ChemPhysChem*, 2018, **19**, 2540–2548.
12 A. Frontera and A. Bauza, *Chemistry*, 2018, **24**, 16582–16587.
13 M. Breugst and J. J. Koenig, *Eur. J. Org. Chem.*, 2020, **2020**, 5473–5487.
14 T. Clark, M. Hennemann, J. S. Murray and P. Politzer, *J. Mol. Model.*, 2007, **13**, 291–296.
15 P. Politzer, J. S. Murray and T. Clark, *Phys. Chem. Chem. Phys.*, 2010, **12**, 7748–7757.
16 S. Scheiner, *Phys. Chem. Chem. Phys.*, 2021, **23**, 5702–5717.
17 M. A. A. Ibrahim, N. A. M. Moussa, A. A. K. Kamel, M. N. I. Shehata, M. N. Ahmed, F. Taha, M. A. S. Abourehab, A. M. Shawky, E. B. Elkaeed and M. E. S. Soliman, *Molecules*, 2022, **27**, 2963.
18 S. Scheiner, *Inorg. Chem. Commun.*, 2020, **59**, 9315–9324.
19 D. Palanisamy, *J. Mol. Model.*, 2020, **26**, 1–15.
20 I. Alkorta, J. Elguero, J. E. Del Bene, O. Mo, M. M. Montero-Campillo and M. Yanez, *J. Phys. Chem. A*, 2020, **124**, 5871–5878.
21 S. J. Grabowski, *Struct. Chem.*, 2019, **30**, 1141–1152.
22 F. U. Rahman, D. Tzeli, I. D. Petsalakis, G. Theodorakopoulos, P. Ballester, J. Rebek and Y. Yu, *J. Am. Chem. Soc.*, 2020, **142**, 5876–5883.
23 V. Kumar, Y. Xu and D. L. Bryce, *Chemistry*, 2020, **26**, 3275–3286.
24 P. C. Ho, J. Z. Wang, F. Meloni and I. Vargas-Baca, *Coord. Chem. Rev.*, 2020, **422**, 213464.
25 M. H. Kolar and P. Hobza, *Chem. Rev.*, 2016, **116**, 5155–5187.
26 Z. Zhu, Z. Xu and W. Zhu, *J. Chem. Inf. Model.*, 2020, **60**, 2683–2696.
27 R. Wang, Q. Li and S. Scheiner, *Appl. Organomet. Chem.*, 2020, **34**, e5891.
28 S. Mondal, D. Manna, K. Raja and G. Mugesh, *ChemBioChem*, 2020, **21**, 911–923.
29 M. D. Esrafili, S. Asadollahi and M. Vakili, *Int. J. Quantum. Chem.*, 2016, **116**, 1254–1260.
30 R. Wang, H. Liu, Q. Li and S. Scheiner, *Phys. Chem. Chem. Phys.*, 2020, **22**, 4115–4121.
31 M. A. A. Ibrahim, M. N. I. Shehata, H. A. A. Abuelliel, N. A. M. Moussa, S. R. M. Sayed, M. N. Ahmed, M. K. Abd El-Rahman, E. Dabbish and T. Shoeib, *R. Soc. Open Sci.*, 2023, **10**, 231362.
32 P. Politzer, J. S. Murray and T. Clark, *Phys. Chem. Chem. Phys.*, 2013, **15**, 11178–11189.
33 A. Bauza and A. Frontera, *Angew. Chem.*, 2015, **54**, 7340–7343.
34 R. Wysokinski, W. Zierkiewicz, M. Michalczyk and S. Scheiner, *ChemPhysChem*, 2022, **23**, e202200173.
35 S. Scheiner, *J. Phys. Chem. A*, 2023, **127**, 9760–9770.
36 W. Zierkiewicz, M. Michalczyk and S. Scheiner, *Phys. Chem. Chem. Phys.*, 2018, **20**, 8832–8841.
37 S. Scheiner and J. Lu, *Chem.–Eur. J.*, 2018, **24**, 8167–8177.
38 M. A. A. Ibrahim, A. M. M. Mahmoud, M. N. I. Shehata, R. R. A. Saeed, N. A. M. Moussa, S. R. M. Sayed, M. K. Abd El-Rahman and T. Shoeib, *ACS Omega*, 2024, **9**, 10391–10399.
39 M. J. Frisch, G. W. Trucks, H. B. Schlegel, G. E. Scuseria, M. A. Robb, J. R. Cheeseman, G. Scalmani, V. Barone, B. Mennucci, G. A. Petersson, H. Nakatsuji, M. Caricato, X. Li, H. P. Hratchian, A. F. Izmaylov, J. Bloino, G. Zheng, J. L. Sonnenberg, M. Hada, M. Ehara, K. Toyota, R. Fukuda, J. Hasegawa, M. Ishida, T. Nakajima, Y. Honda, O. Kitao, H. Nakai, T. Vreven, J. A. Montgomery, J. E. Peralta, F. Ogliaro, M. Bearpark, J. J. Heyd, E. Brothers, K. N. Kudin, V. N. Staroverov, R. Kobayashi, J. Normand, K. Raghavachari, A. Rendell, J. C. Burant, S. S. Iyengar, J. Tomasi, M. Cossi, N. Rega, J. M. Millam, M. Klene, J. E. Knox, J. B. Cross, V. Bakken, C. Adamo, J. Jaramillo, R. Gomperts, R. E. Stratmann, O. Yazyev, A. J. Austin, R. Cammi, C. Pomelli, J. W. Ochterski, R. L. Martin, K. Morokuma, V. G. Zakrzewski, G. A. Voth, P. Salvador, J. J. Dannenberg, S. Dapprich, A. D. Daniels, Ö. Farkas, J. B. Foresman, J. V. Ortiz, J. Cioslowski and D. J. Fox, *Gaussian 09 Revision E01*, Gaussian Inc., Wallingford CT, USA, 2009.
40 C. Møller and M. S. Plesset, *Phys. Rev.*, 1934, **46**, 618–622.
41 D. E. Woon and T. H. Dunning, *J. Chem. Phys.*, 1993, **98**, 1358–1371.
42 D. E. Woon and T. H. Dunning, *J. Chem. Phys.*, 1994, **100**, 2975–2988.
43 K. A. Peterson, D. Figgen, E. Goll, H. Stoll and M. Dolg, *J. Chem. Phys.*, 2003, **119**, 11113–11123.
44 K. A. Peterson, B. C. Shepler, D. Figgen and H. Stoll, *J. Phys. Chem. A*, 2006, **110**, 13877–13883.
45 C. H. Suresh, G. S. Remya and P. K. Anjalikrishna, *Wiley Interdiscip. Rev.:Comput. Mol. Sci.*, 2022, **12**, e1601.

46 N. Mohan and C. H. Suresh, *J. Phys. Chem. A*, 2014, **118**, 1697–1705.
47 C. H. Suresh and S. Anila, *Acc. Chem. Res.*, 2023, **56**, 1884–1895.
48 M. A. A. Ibrahim, *J. Mol. Model.*, 2012, **18**, 4625–4638.
49 P. K. Weiner, R. Langridge, J. M. Blaney, R. Schaefer and P. A. Kollman, *Proc. Natl. Acad. Sci. U. S. A.*, 1982, **79**, 3754–3758.
50 M. A. A. Ibrahim, R. R. A. Saeed, M. N. I. Shehata, E. E. B. Mohamed, M. E. S. Soliman, J. H. Al-Fahemi, H. R. A. El-Mageed, M. N. Ahmed, A. M. Shawky and N. A. M. Moussa, *J. Mol. Struct.*, 2022, **1265**, 133232.
51 M. A. A. Ibrahim, M. N. I. Shehata, A. S. M. Rady, H. A. A. Abuelliel, H. S. M. Abd Elhafez, A. M. Shawky, H. F. Oraby, T. H. A. Hasanin, M. E. S. Soliman and N. A. M. Moussa, *Int. J. Mol. Sci.*, 2022, **23**, 13023.
52 L. Piela, *Ideas of Quantum Chemistry*, Elsevier, 2006.
53 S. J. Grabowski and W. A. Sokalski, *J. Phys. Org. Chem.*, 2005, **18**, 779–784.
54 S. F. Boys and F. Bernardi, *Mol. Phys.*, 1970, **19**, 553–566.
55 B. K. Mishra, S. Karthikeyan and V. Ramanathan, *J. Chem. Theory Comput.*, 2012, **8**, 1935–1942.
56 A. Halkier, W. Klopper, T. Helgaker, P. Jorgensen and P. R. Taylor, *J. Chem. Phys.*, 1999, **111**, 9157–9167.
57 R. F. W. Bader, *Acc. Chem. Res.*, 1985, **18**, 9–15.
58 E. R. Johnson, S. Keinan, P. Mori-Sanchez, J. Contreras-Garcia, A. J. Cohen and W. Yang, *J. Am. Chem. Soc.*, 2010, **132**, 6498–6506.
59 T. Lu and F. Chen, *J. Comput. Chem.*, 2012, **33**, 580–592.
60 W. Humphrey, A. Dalke and K. Schulten, *J. Mol. Graphics*, 1996, **14**, 33–38.
61 T. M. Parker, L. A. Burns, R. M. Parrish, A. G. Ryno and C. D. Sherrill, *J. Chem. Phys.*, 2014, **140**, 094106.
62 E. G. Hohenstein and C. D. Sherrill, *J. Chem. Phys.*, 2010, **132**, 184111.
63 J. M. Turney, A. C. Simmonett, R. M. Parrish, E. G. Hohenstein, F. A. Evangelista, J. T. Fermann, B. J. Mintz, L. A. Burns, J. J. Wilke, M. L. Abrams, N. J. Russ, M. L. Leininger, C. L. Janssen, E. T. Seidl, W. D. Allen, H. F. Schaefer, R. A. King, E. F. Valeev, C. D. Sherrill and T. D. Crawford, *Wiley Interdiscip. Rev.:Comput. Mol. Sci.*, 2012, **2**, 556–565.
64 J. Zurita, V. Rodriguez, C. Zambrano, J. R. Mora, L. Rincón and F. J. Torres, *Molecules*, 2020, **25**, 530.
65 A. D. Becke and K. E. Edgecombe, *J. Chem. Phys.*, 1990, **92**, 5397–5403.
66 M. A. A. Ibrahim, R. R. A. Saeed, M. N. I. Shehata, N. A. M. Moussa, A. M. Tawfeek, M. N. Ahmed, M. K. Abd El-Rahman and T. Shoeib, *ACS Omega*, 2023, **8**, 32828–32837.
67 W. D. Arnold and E. Oldfield, *J. Am. Chem. Soc.*, 2000, **122**, 12835–12841.
68 B. Jeziorski, R. Moszynski and K. Szalewicz, *Chem. Rev.*, 1994, **94**, 1887–1930.
69 M. A. A. Ibrahim and A. A. M. Hasb, *Theor. Chem. Acc.*, 2019, **138**, 2–13.